

Dynamical behavior of ring-star neural networks with small-world characteristics

Minglin Ma(马铭磷), Zhiyi Yuan(袁芷依), Umme Kalsoom, Weizheng Deng(邓为政), and Shaobo He(贺少波)
Citation: Chin. Phys. B, 2025, 34 (**10**): 100502. DOI: 10.1088/1674-1056/adde39
http://cpb.iphy.ac.cn; http://iopscience.iop.org/cpb

What follows is a list of articles you may be interested in

Design of a memristive chaotic map and its adaptive regulation

Ya Wang(王亚), Xin-Lin Song(宋欣林), and Fei-Fei Yang(杨飞飞)
Chin. Phys. B, 2025, 34 (**9**): 090504. DOI: 10.1088/1674-1056/adea5c

Dynamical behaviors of a multifunctional neural circuit

Xiao-Hong Gao(高晓红), Kai-Long Zhu(朱凯龙), and Fei-Fei Yang(杨飞飞)
Chin. Phys. B, 2025, 34 (**9**): 090503. DOI: 10.1088/1674-1056/ae001b

A novel non-autonomous hyperchaotic map based on discrete memristor parallel connection

Weiping Wu(吴伟平), Mengjiao Wang(王梦蛟), and Qigui Yang(杨启贵)
Chin. Phys. B, 2025, 34 (**5**): 050503. DOI: 10.1088/1674-1056/adb8bc

Dynamics and synchronization of neural models with memristive membranes under energy coupling

Jingyue Wan(万婧玥), Fuqiang Wu(吴富强), Jun Ma(马军), and Wenshuai Wang(汪文帅)
Chin. Phys. B, 2024, 33 (**5**): 050504. DOI: 10.1088/1674-1056/ad1dcc

Fractional-order heterogeneous memristive Rulkov neuronal network and its medical image watermarking application

Dawei Ding(丁大为), Yan Niu(牛炎), Hongwei Zhang(张红伟), Zongli Yang(杨宗立), Jin Wang(王金), Wei Wang(王威), and Mouyuan Wang(王谋媛)
Chin. Phys. B, 2024, 33 (**5**): 050503. DOI: 10.1088/1674-1056/ad322b

---

Dynamical behavior of ring-star neural networks with small-world characteristics

Minglin Ma(马铭磷)[1], Zhiyi Yuan(袁芷依)[1], Umme Kalsoom[2], Weizheng Deng(邓为政)[1], and Shaobo He(贺少波)[1,†]

[1] *School of Automation and Electronic Information, Xiangtan University, Xiangtan* 411105, *China*
[2] *Department of Computer Science University of Narowal, Pakistan*

(Received 6 May 2025; revised manuscript received 23 May 2025; accepted manuscript online 29 May 2025)

This paper proposes a ring-star neural network with small-world characteristics (RS-SWNN) based on the classical ring-star network, and combines the Izhikevich neuron model. RS-SWNN incorporates small-world characteristics, better mimicking the non-uniform connectivity of biological neural networks. According to the different coupling strength settings of D_{ring} and D_{star}, the dynamical behavior of the network is studied, and the synchronicity differences of the network under different coupling strengths are revealed. In addition, a discrete memristor is used to simulate the effects of electromagnetic radiation. The modulation effects of varying radiation intensities on the network synchronization are further analyzed. The study shows that the electromagnetic radiation effect significantly impacts the neuronal synchronization behavior, especially in its modulation of network synchronization under varying coupling strengths. Numerical simulation is carried out using MATLAB software, and the corresponding results are obtained.

Keywords: Izhikevich neurons, memristor, synchronization, electromagnetic radiation

PACS: 05.45.Xt, 87.85.dq, 05.45.–a, 05.90.+m

DOI: 10.1088/1674-1056/adde39 **CSTR:** 32038.14.CPB.adde39

1. Introduction

The study of neuronal behavior is crucial, as neurons serve as the essential components of the brain and are the core units of information transmission.[1–3] An ideal neuronal model should be able to describe various bursting and spiking characteristics while maintaining high computational efficiency, especially when simulating large numbers of neurons, as this is key to modeling large-scale neural networks. The Hodgkin–Huxley model was one of the earliest neuronal models to achieve this goal.[4] It successfully simulates the physiological properties of neurons by describing the dynamics of ion channels. However, the model's computational complexity is high, which poses challenges in large-scale neural network simulations due to the computational cost. To tackle this problem, Izhikevich proposed a simplified neuronal model[5] that can mimic the behavior of numerous neurons quickly while still retaining biological accuracy. This model not only simulates various neuronal firing patterns,[6] such as regular spiking, intrinsic bursting, and tremor firing, but also effectively describes the behavior of thalamocortical neurons, exhibiting spiking and bursting characteristics similar to those of biological neurons. Vivekanandhan *et al.*[7] proposed an improved neuron model by incorporating an electric field into the Izhikevich neuron model. By varying the parameters, they investigated the dynamic behavior of the model. Experimental results demonstrated that the presence of the electric field leads to complete synchronization at higher coupling coefficients. Aristides *et al.*[8] investigated the linear stability of synchronization states in Izhikevich neuron networks using the master stability function (MSF). Faci-Lázaro *et al.*[9] employed the Izhikevich neuron model to describe network dynamical behavior, revealing the activation patterns of neuronal networks. Overall, the Izhikevich neuron model is widely used in neural network research and dynamical analysis of the nervous system due to its computational efficiency and biological realism.

The memristor was first proposed by Leon Chua in 1971[10] and was physically realized in 2008.[11] In the context of neural networks, memristors not only effectively simulate synapses in biological neural systems[12–15] but can also be used to model electromagnetic radiation induction phenomena.[16–19] Yu *et al.*[20] constructed a memristive tri-neuron Hopfield neural network (MTN-HNN), in which the synapse of the second neuron was replaced by the proposed memristor, and conducted theoretical and experimental studies on the dynamics of this neural network. Wang *et al.*[21] designed a new type of discrete memristor, connected the Chialvo model, constructed a two-neuron coupled system and a two-dimensional lattice neural network, and analyzed the synchronization and spatiotemporal dynamics of the neural network. A new neuromorphic architecture, proposed by Deng *et al.*,[22] integrates memristors with piecewise nonlinear dynamics into tabu learning neuron circuits, thus forming an innovative memristive tabu learning neuron model that can produce two-winged chaotic butterflies. With further optimization of memristor technology, its prospects in applications such as

†Corresponding author. E-mail: heshaobo@xtu.edu.cn

© 2025 Chinese Physical Society and IOP Publishing Ltd. All rights, including for text and data mining, AI training, and similar technologies, are reserved.

neural networks, image encryption,[23,24] and circuit system design are very promising.

The neural network simulates the process of information transmission and processing between neurons in the biological brain.[25–28] The synchronization of the neural network refers to the coordinated firing activity of multiple neurons in the network. Synchronization plays a crucial role in biological neural systems.[29–32] In Ref. [33], the authors study the impact of modifying system parameters on the synchronization characteristics of the dual-attribute ring-star neural network (DRSNN). In Ref. [34], based on the Rulkov neuron model, a scale-free neural network model with heterogeneous time delays is designed, called the heterogeneous scale-free neural network (HSFNN), and its dynamic behavior was studied. In Ref. [35], the authors show the dynamic transition from a simple network of two coupled systems to a network of nodes, demonstrating synchronicity with increasing coupling strength for all network connections. In Ref. [36], to study the impact of network heterogeneity on neuronal synchronization, a small-world network consisting of electrically coupled non-identical Chialvo neurons was analyzed. By deeply studying the synchronization mechanism of neuronal networks, we can not only deepen our understanding of brain function but also form vital foundations for developing diagnostic tools and treatment strategies.[37,38]

In the brain's neural network, the rhythmic oscillations of neuronal electrical potentials induce time-varying electromagnetic fields, which subsequently exert regulatory effects on the very electrophysiological properties that initiated them.[39] Reference [40] introduces the impact of electromagnetic radiation into scale-free neural networks. The research shows that under appropriate electromagnetic radiation intensity, a neural network can achieve good synchronization. Njitacke *et al*. studied the impact of electromagnetic flux on the dynamics of the introduced heterogeneous coupled neuron model.[41] Reference [42] systematically studied the dynamic behavior of an improved discrete Izhikevich neuron model exposed to external electromagnetic stimulation, and the impact of electromagnetic radiation on the ring-star neural network model of the Izhikevich neuron was also considered. In Ref. [43], a small-world neural network with electrical synaptic connections was constructed, and the inverse stochastic resonance of the small-world neural network under electromagnetic radiation stimulation was investigated by analyzing the dynamics of the neural network.

However, neuronal connections in real brain neural networks exhibit complex topological structures that lie between regular and random. Based on these considerations, this paper proposes a more biologically plausible network model — the ring-star neural network model with small-world properties (RS-SWNN). The main contributions of this paper are as follows: 1) A new RS-SWNN is proposed to simulate the neuron connections in real brain neural networks. 2) The effect of coupling strength on the dynamic performance of RS-SWNNs in three modes is studied. 3) The influence of electromagnetic radiation induction intensity on the dynamic behavior of RS-SWNNs.

The article is structured in the following manner. Section 2 establishes the model, detailing the discrete memristor model and the RS-SWNN model based on Izhikevich neurons. Section 3 examines the correlation between the coupling strength and the dynamic behavior of the RS-SWNN, as well as the impact of electromagnetic radiation induction on the RS-SWNN's dynamics. Section 4 presents the conclusions.

2. Model construction

2.1. Discrete memristor model

This study uses memristors to simulate electromagnetic induction effects based on the four-state discrete memristor outlined in Ref. [40]. The discrete memristor framework is detailed below:

$$\begin{cases} i(n) = W(\phi(n))v(n) = \phi(n)v(n), \\ \phi(n+1) = 0.1(\mathrm{sgn}(\phi(n)) + \mathrm{sgn}(\phi(n+2)) \\ \quad + \mathrm{sgn}(\phi(n-2)) - \phi(n)) + \phi(n) + 0.01v(n). \end{cases} \tag{1}$$

Here, $i(n)$ signifies the current, $v(n)$ denotes the voltage, $W(\phi(n))$ stands for the memductance, and $\phi(n)$ indicates the internal state of the memristor.

2.2. RS-SWNN model

To reflect the heterogeneity of neural networks, we constructed an RS-SWNN. We introduce discrete Izhikevich neurons as the nodes of the network while using discrete memristors to simulate electromagnetic radiation. The model consists of 200 nodes, with node 1 serving as the central node and the remaining nodes as peripheral ones. The mathematical representation of peripheral nodes is as follows ($i \in [2, 200]$):

$$\begin{cases} v_i(t+1) = v_i(t) + 0.04v_i(t)^2 + 5v_i(t) + 140 - u_i(t) + I \\ \qquad + D_{\mathrm{star}}\varepsilon_{1,i}(v_1(t) - v_i(t)) + D_{\mathrm{ring}}\sum_{j=2}\varepsilon_{i,j}(v_j(t) - v_i(t)) + k\phi_i(t)v_i(t), \\ u_i(t+1) = u_i(t) + a(bv_i(t) - u_i(t)), \\ \text{if } v_i(t+1) \geq 30 \begin{cases} v_i(t+1) \leftarrow c, \\ u_i(t+1) \leftarrow u + d, \end{cases} \\ \phi_i(t+1) = 0.1(\mathrm{sgn}(\phi_i(t)) + \mathrm{sgn}(\phi_i(t)+2) + \mathrm{sgn}(\phi_i(t)-2) - \phi_i(t)) + \phi_i(t) + 0.01v_i(t). \end{cases} \tag{2}$$

The central node can be described as follows:

$$\begin{cases} v_1(t+1) = v_1(t) + 0.04v_1(t)^2 + 5v_1(t) + 140 - u_1(t) + I + D_{\text{star}} \sum_j \varepsilon_{1,j} \left(v_j(t) - v_1(t)\right) + k\phi_1(t)v_1(t), \\ u_1(t+1) = u_1(t) + a\left(bv_1(t) - u_1(t)\right), \\ \text{if } v_1(t+1) \geq 30 \begin{cases} v_1(t+1) \leftarrow c, \\ u_1(t+1) \leftarrow u + d, \end{cases} \\ \phi_1(t+1) = 0.1\left(\text{sgn}\left(\phi_1(t)\right) + \text{sgn}\left(\phi_1(t) + 2\right) + \text{sgn}\left(\phi_1(t) - 2\right) - \phi_1(t)\right) + \phi_1(t) + 0.01v_1(t). \end{cases} \tag{3}$$

Equation (2) consists of two coupling terms: D_{ring} and D_{star}. They are the coupling strength among peripheral nodes and the coupling strength between the central node and peripheral nodes. Here, v_i represents the membrane voltage (in millivolts), and u_i is the recovery variable. The variables a, b, c, and d are dimensionless parameters, and I represents the external input current. The reset of the state variables is as follows: if $v \geq 30$ mV, then $u \rightarrow u + d$, and $v \rightarrow c$. $\varepsilon_{i,j}$ is the connection matrix, which determines whether a connection is established between nodes, while k represents the intensity of electromagnetic radiation. Equation (3) describes the dynamic behavior of the central node. Due to the unique position of the central node, it includes only the D_{star} term.

The ring-star network is a relatively unique and complex network model that combines the advantages of star topology and ring topology, forming a distinctive network structure. In a traditional star network, all nodes are connected through a central node, with all data transmission relying on the central node. In contrast, in a ring network, nodes are interconnected in a ring-like structure, forming a closed loop, where data is transmitted along the ring, with each node forwarding to the next node. The ring-star network merges these two structures by linking the central node to the nodes within the ring configuration. This leverages the centralized control of the central node to simplify management while enhancing redundancy and fault tolerance through the ring structure.

Figure 1[42] illustrates a schematic diagram of a ring-star network consisting of N nodes. In this network, the outer ring structure is composed of $N-1$ nodes. Each outer node is connected not only to its immediate neighbors on the left and right but also to a node in the central star topology.

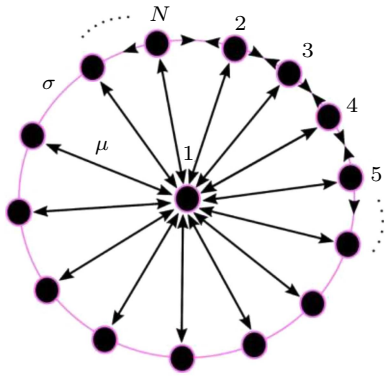


Fig. 1. Schematic diagram of the ring-star network.

Figure 2 illustrates the modified ring-star network model. In this model, some regular connections from the classical ring-star network are removed; thus, the RS-SWNN model is constructed.

As shown in Fig. 2, the red lines represent the original regular connections in the ring-star network, while the blue lines indicate newly added connections after disconnection and reconnection. Specifically, we disconnect and reconnect the nodes on the ring network with a probability of $P_1 = 0.1$. That is, we randomly disconnect a node from one of its adjacent nodes and establish a new connection with another random node within the ring. This process disrupts the original local regular connection structure, thereby imparting typical small-world characteristics to the ring network. Meanwhile, with a probability of $P_2 = 0.2$, we randomly disconnect the connections between the central node and the peripheral nodes, reducing the central node's absolute control over the network and ensuring that the central node no longer directly connects to all peripheral nodes. Some peripheral nodes can interact through the central node, while others can interact directly with each other. Through these steps, the model retains the important role of the central node while enhancing the flexibility of interactions among the peripheral nodes.

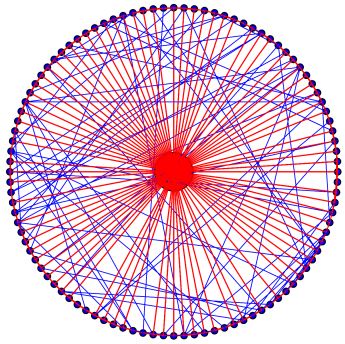


Fig. 2. Schematic diagram of the RS-SWNN.

3. Dynamical behavior analysis of the RS-SWNN

The dynamic behavior of the RS-SWNN can be controlled by adjusting the coupling strength parameters to achieve three typical working modes. Mode-I (ring-dominated coupling) only considers the coupling between peripheral nodes ($D_{\text{ring}} \neq 0$, $D_{\text{star}} = 0$), and the influence of the central

node is ignored. Mode-II (star-dominant coupling) only considers the coupling between the central node and the peripheral nodes ($D_{\text{star}} \neq 0$, $D_{\text{ring}} = 0$), the direct interaction between the peripheral nodes is ignored, and the control of the entire network by the central node becomes the dominant feature. Mode-III (hybrid coupling) considers both the coupling between the central node and the peripheral nodes and the interaction between the peripheral nodes ($D_{\text{star}} \neq 0$, $D_{\text{ring}} \neq 0$). The remaining system parameters are distributed as follows: $d = 2$, $c = -55$, $b = 0.25$, $a = 0.02$, and $I = 1$.

3.1. Influence of coupling strength on synchronization

3.1.1. Dynamic behavior of the RS-SWNN in mode-I

In this section, we consider only the influence of coupling strength on the network, with the electromagnetic radiation intensity set to $k = 0$. In neural networks, it is generally believed that network synchronization increases monotonically with coupling strength. However, in the mode-I RS-SWNN, the degree of synchronization does not exhibit a monotonic increase as D_{ring} increases. As shown in Fig. 3, we record the dynamic behavior of the RS-SWNN in mode-I at D_{ring} values of 0.001, 0.008, and 0.065. Figure 3(a) shows the spatiotemporal diagram of the RS-SWNN in mode-I at $D_{\text{ring}} = 0.001$. It can be observed that when the coupling strength is low, the firing differences between neurons remain small, and the synchronization of the network is not completely disrupted. Figure 3(b) records the firing moments of all neurons in the network, where each point represents a neuron's firing instance, clearly reflecting that most neurons exhibit minimal differences in firing times. Figure 3(c) provides a visualization based on Fig. 3(b). Specifically, we calculate the time difference for each firing event across all neurons, then compute the overall average to obtain a differential heat map of firing moments. When all neurons fire at the same moment, indicating a fully synchronized state, the firing time differences are zero, and the corresponding differential heat map of firing moments appears dark blue. When D_{ring} increases to 0.008, it can be observed from Figs. 3(d)–3(f) that the synchronization of the network is significantly disrupted compared to the previous state. The firing times of neurons become more dispersed, indicating a decline in overall network synchronization. The enhanced interactions between neurons produce destructive interference with the original firing pattern. As D_{ring} increases, instead of improving synchronization, the network exhibits greater irregularity. When $D_{\text{ring}} = 0.065$, the network exhibits strong synchronization characteristics. As shown in Figs. 3(g)–3(i), the firing times of all peripheral nodes, except for the central node (node 1), align almost perfectly along a single trajectory, demonstrating a clear synchronization pattern. Additionally, the network exhibits a chimera state, where some nodes display synchronization while the central node maintains independent behavior.

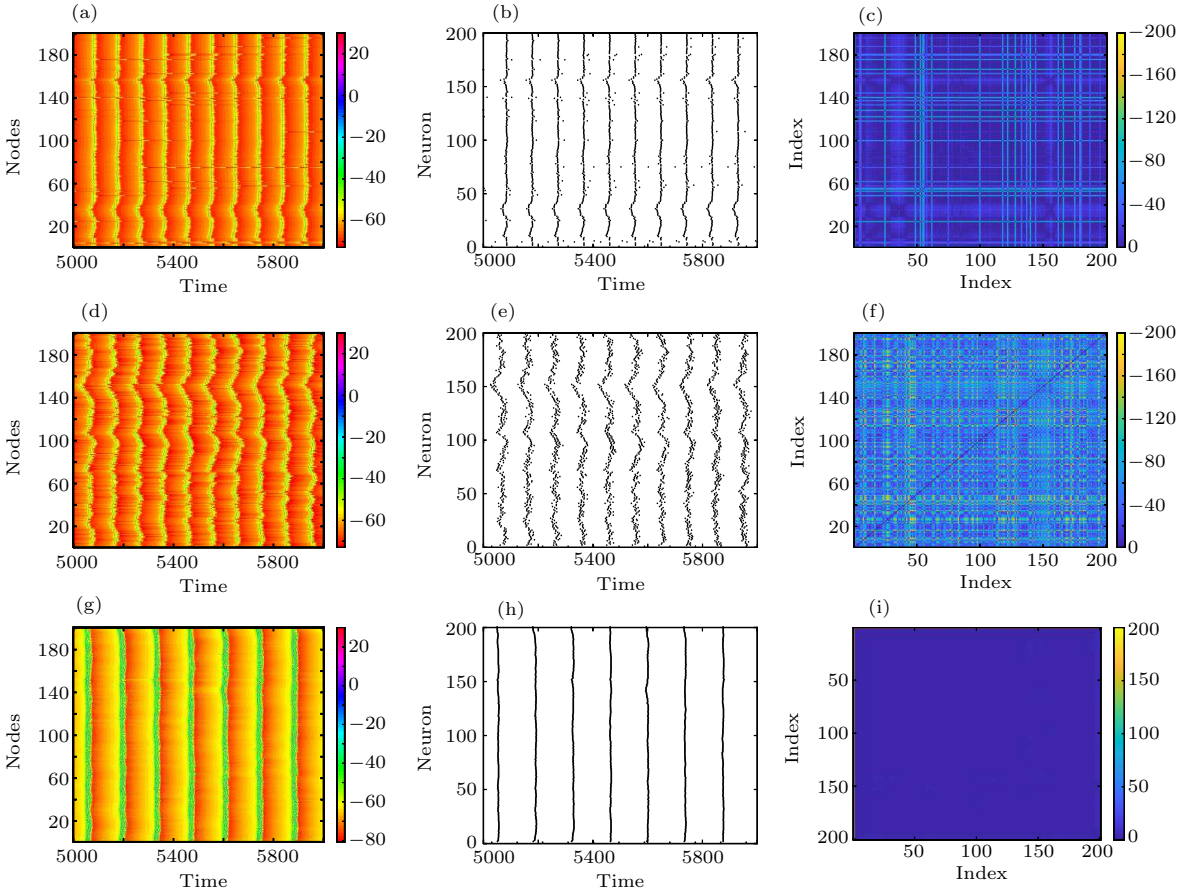


Fig. 3. Spatiotemporal diagrams (left), firing moments (middle), and heat map of firing moment differences (right) for coupling strengths $D_{\text{star}} = 0$, D_{ring} of 0.001, 0.008, and 0.065.

In summary, in mode-I of the RS-SWNN, during the initial stage when the coupling strength D_{ring} is weak, it is insufficient to affect the firing behavior of neurons. Each neuron fires independently based on its dynamical characteristics, and the network maintains good synchronization. In the transitional stage, as D_{ring} increases, neurons begin to influence each other through coupling interactions. The coupling strength is not yet strong enough to control the firing frequency of other neurons, but it is sufficient to disrupt their original frequencies, leading to a deterioration in synchronization. When D_{ring} reaches an appropriate strength, the coupling between neurons becomes strong enough to overcome the differences in individual dynamical properties. Neurons gradually become "locked" into a unified firing rhythm through coupling interactions, and the network exhibits good synchronization. In comparison, as D_{ring} increases, the synchronicity of ordinary ring-star neural networks decreases monotonically, and non-monotonic synchronization does not occur.

3.1.2. Dynamical behavior of the RS-SWNN in mode-II

Next, we consider the effect of the coupling strength D_{star} on the dynamics of the RS-SWNN in mode-II. As shown in Fig. 4, the dynamic behavior of the RS-SWNN in mode-II is recorded for D_{star} values of 0.001, 0.008, and 0.01. Similarly, by fixing D_{star}, it is observed that compared to the case with $D_{\text{star}} = 0.001$, the network synchronization is worse. As shown in Figs. 4(a)–4(c), the RS-SWNN in mode-II still exhibits characteristics of a chimera state, with partial synchronization observed in some regions of the network. For example, local synchronization is evident between nodes 140 to 160 and nodes 15 to 35. As D_{star} continues to increase, the dynamical characteristics of the RS-SWNN in mode-II begin to show significant differences compared to the RS-SWNN in mode-I. As shown in Figs. 4(d)–4(i), the synchronization of the RS-SWNN in mode-II exhibits a monotonic change, with synchronization continuously decreasing. When $D_{\text{star}} = 0.01$, the synchronicity of the network is further weakened, the chimeric state disappears, and the network presents an asynchronous state.

In summary, with a small D_{star}, the interaction between the central node and the peripheral nodes is insufficient to fully dominate the overall behavior of the network. The RS-SWNN in mode-II shows a complex dynamic state of partial synchronization and asynchronous coexistence. As D_{star} increases further, it only serves to continuously disrupt the original firing behavior of neurons, but unlike D_{ring}, it is unable to allow neurons to adjust their firing patterns to re-establish new firing behaviors and achieve synchronization.

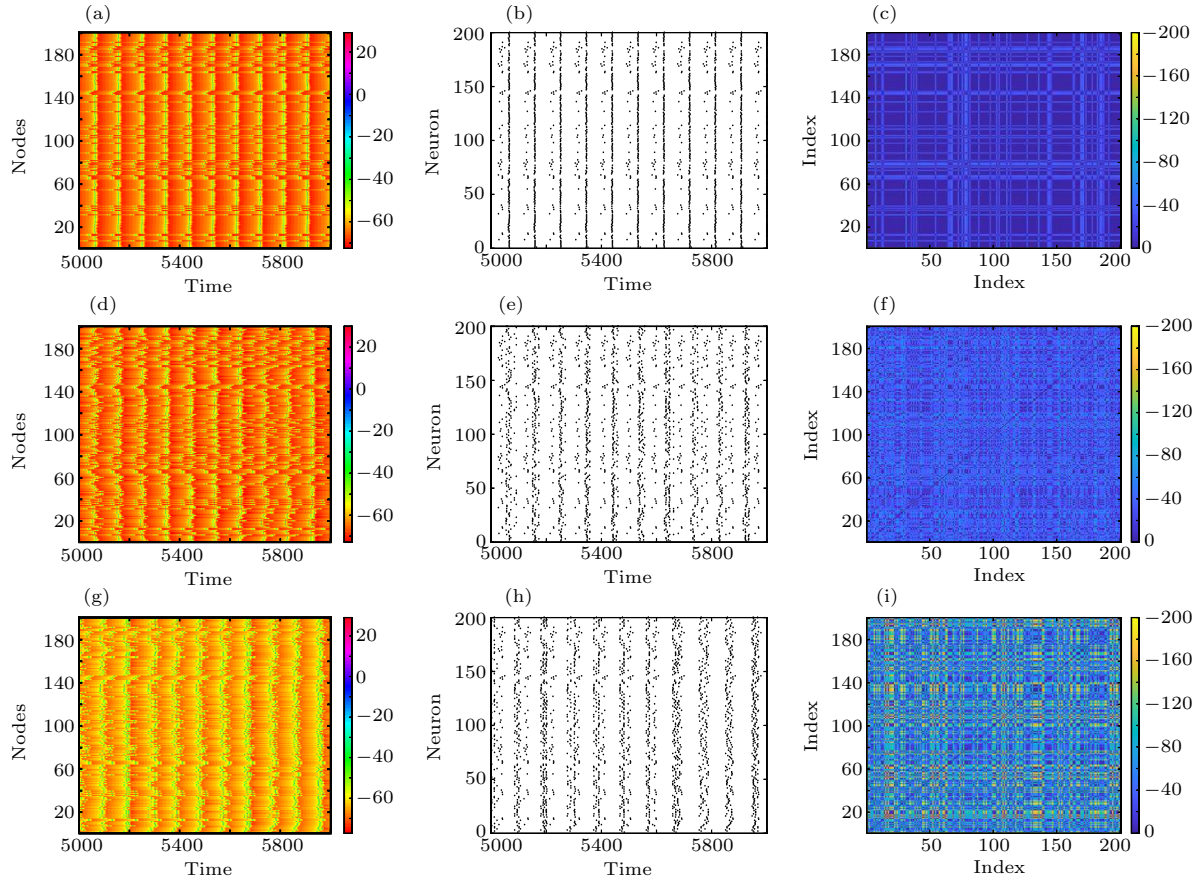


Fig. 4. Spatiotemporal diagrams (left), firing moments (middle), and heat map of firing moment differences (right) for coupling strengths $D_{\text{ring}} = 0$, D_{star} of 0.001, 0.008, and 0.01.

3.1.3. Dynamical behavior of the RS-SWNN in mode-III

Figure 5 records the dynamic behavior of the RS-SWNN in mode-III under the fixed condition $D_{\text{star}} = 0.01$ for different values of D_{ring}. When $D_{\text{ring}} = 0.001$, as shown in Figs. 5(a)–5(c), the strong coupling strength D_{star} between the central node and the peripheral nodes exerts a significant controlling effect on the peripheral nodes, and the entire network is asynchronous. However, when D_{ring} increases to 0.015, as shown in Figs. 5(d)–5(f), a significant improvement in the synchronization of the network can be observed. The increased coupling between peripheral nodes can enhance the interaction between local nodes, allowing peripheral nodes to overcome the control effect from the central node and ultimately show good synchronization. This change shows that although the strong coupling effect (D_{star}) of the central node will destroy the synchronization of the network in the initial stage, as D_{ring} continues to increase, the synchronization of the network shows a monotonically increasing trend.

The above results indicate that in the RS-SWNN in mode-III, the coupling strength among peripheral nodes, D_{ring}, plays a crucial role in regulating network synchronization behavior. Appropriately enhancing the mutual coupling between peripheral nodes can effectively counteract the disruptive effect of the central node on network synchronization, thereby promoting the entire network to achieve a highly synchronized state.

Table 1 summarizes the influence of coupling strength on the synchronization behavior of the RS-SWNN in three modes. In mode-I, ring coupling needs to reach a threshold strength to re-establish synchronization, showing the "destruction-reconstruction" nonlinear characteristics. In mode-II, the enhancement of star coupling only destroys synchronization, and synchronization cannot be restored by adjusting D_{star}. In mode-III, coupling between peripheral nodes is a key factor to break the control of the central node and achieve global synchronization.

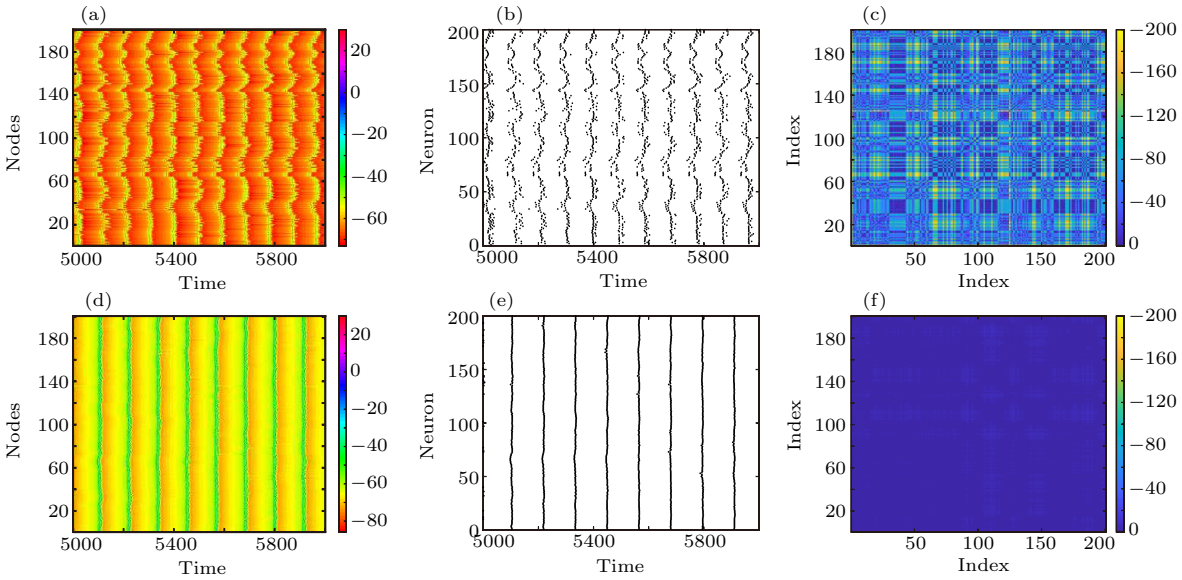


Fig. 5. Spatiotemporal diagrams (left), firing moments (middle), and heat map of firing moment differences (right) for coupling strengths $D_{\text{star}} = 0.01$ and $D_{\text{ring}} = 0.001, 0.015$.

Table 1. Impact of coupling strength on RS-SWNN synchronization.

Mode	Coupling parameters	Observations & conclusions
Mode-I	$D_{\text{ring}} \uparrow D_{\text{star}} = 0$	$D_{\text{ring}} = 0.001$, network maintains good synchronization.
		$D_{\text{ring}} = 0.008$, synchronization deteriorates.
		$D_{\text{ring}} = 0.065$, network resynchronizes; central node independence.
Mode-II	$D_{\text{star}} \uparrow D_{\text{ring}} = 0$	$D_{\text{star}} = 0.001$, partial synchronization coexists with asynchrony (chimera state).
		$D_{\text{star}} \uparrow (0.008–0.01)$, synchronization monotonically declines, leading to complete asynchrony.
Mode-III	$D_{\text{star}} = 0.01$ $D_{\text{ring}} \uparrow$	$D_{\text{ring}} = 0.001$, strong central node control results in network asynchrony.
		$D_{\text{ring}} = 0.015$, enhanced peripheral coupling counteracts central node interference, significantly improving synchronization.

3.2. The influence of electromagnetic radiation on synchronization

To make the RS-SWNN more representative of the real working environment of the brain, a global electromagnetic radiation effect is introduced, allowing all neurons to be influenced by electromagnetic radiation. Since the impact of electromagnetic radiation is similar in the RS-SWNN in mode-II, mode-I, and mode-III, this section presents only the dynamic behavior of the RS-SWNN in mode-I under different electromagnetic radiation intensities k.

With the coupling strength fixed at $D_{\text{ring}} = 0.001$ and the electromagnetic radiation intensity set to $k = 0.001$, a comparison between Figs. 6(a), 6(b) and 3(a)–3(c) reveals that the electromagnetic radiation effect can significantly disrupt network synchronization. Despite the small k value, the electromagnetic radiation is sufficient to disturb the original firing rhythm of neurons, causing the network to exhibit more disordered dynamical behavior. When the electromagnetic radiation intensity increases to $k = 0.01$, as shown in Figs. 6(c) and 6(d), the network remains in an asynchronous state. However, compared to the case of $k = 0.001$, the firing frequency of neurons increases significantly, exhibiting higher activity. This indicates that as the electromagnetic radiation intensity strengthens, network synchronization does not improve, but individual neuronal firing becomes more frequent due to stimulation.

In summary, the experimental results demonstrate that the electromagnetic radiation effect has a significant impact on the dynamical behavior of the RS-SWNN in mode-I. Even at relatively small k values, it can disrupt network synchronization, while stronger electromagnetic radiation enhances the firing frequency of individual neurons.

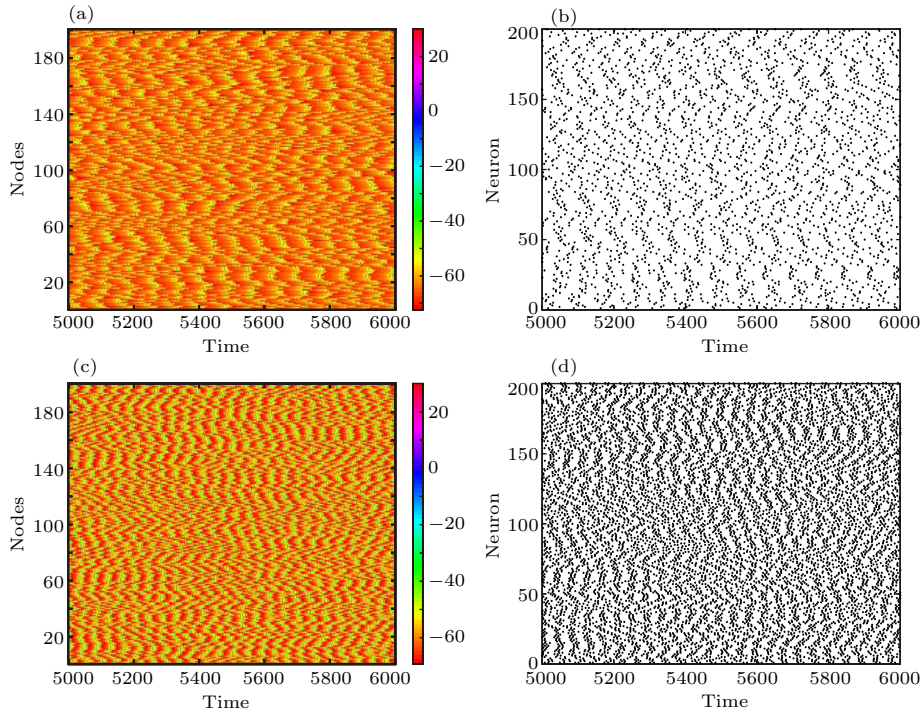


Fig. 6. Spatiotemporal diagrams (left) and firing times (right) for $D_{\text{star}} = 0$, $D_{\text{ring}} = 0.001$ under electromagnetic radiation intensities $k = 0.001$ and $k = 0.01$.

When D_{ring} increases to 0.008 and $k = 0.001$, as shown in Figs. 7(a) and 7(b), a comparison with Figs. 3(d) and 3(e) reveals that the RS-SWNN in the mode-I model exhibits similar dynamical behavior to the case without electromagnetic radiation, with poor network synchronization. However, when k increases to 0.008, an interesting phenomenon appears in Figs. 7(c) and 7(d): the network shows good synchronization, with almost all neurons' firing times aligning. This is different from the phenomenon observed when $D_{\text{ring}} = 0.001$ and $k = 0.01$.

The electromagnetic radiation intensity k has a significant modulatory effect on the synchronization of the RS-SWNN in mode-I. Under the fixed coupling strength $D_{\text{ring}} = 0.008$, when k increases, the synchronization of the network is significantly enhanced. In comparison, as k increases in the ordinary star ring network, the synchronization of the network does not increase.

To further explore the effects of electromagnetic radiation, we increased the coupling strength to $D_{\text{ring}} = 0.065$. When electromagnetic radiation is introduced at $k = 0.001$, a comparison with Figs. 3(g) and 3(h) reveals that the RS-SWNN in the mode-I model exhibits similar dynamical behavior to the case without electromagnetic radiation. As shown in Figs. 8(a) and 8(b), the spatiotemporal diagram displays a uniform color distribution, and in the firing time diagram, neuron firing times form distinct stripe-like patterns, indicating that nearly all neurons fire synchronously. This suggests that under strong ring coupling, the network has entered a highly synchronized and stable state. This behavior is entirely different from the case where $D_{\text{ring}} = 0.001$, in which network synchronization is severely disrupted under the same electromagnetic radiation intensity of $k = 0.001$ (see Figs. 6(a) and 6(b)). When k is further increased to 0.008, as shown in Figs. 8(c) and 8(d), the increase in k not only leads to a higher firing frequency of neurons but does not produce any significant changes in the overall synchronization of the RS-SWNN in mode-I.

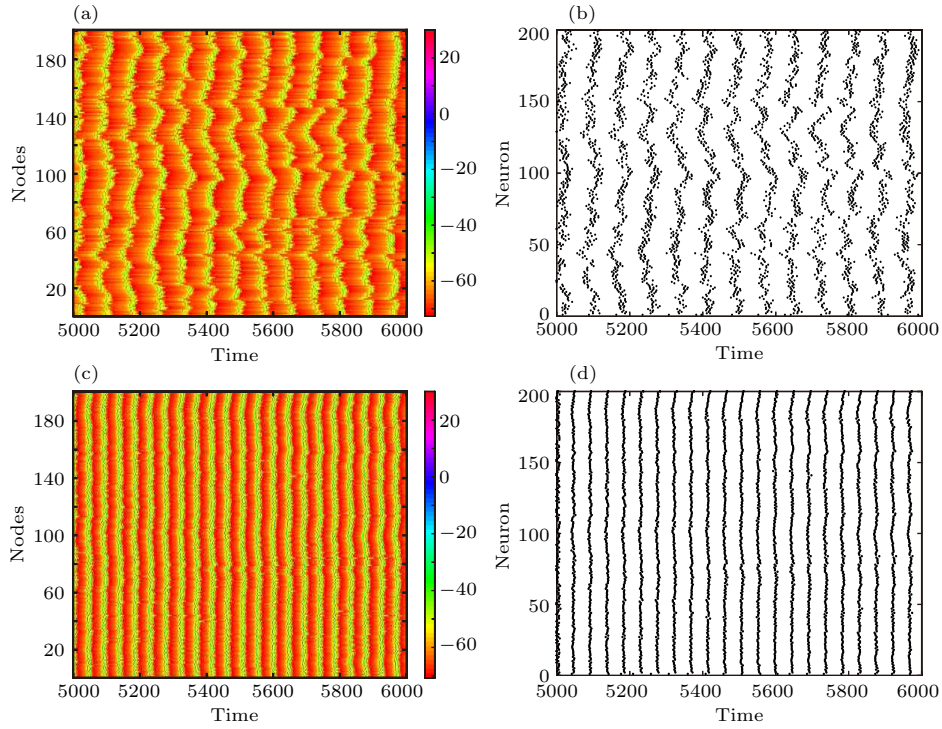


Fig. 7. Spatiotemporal diagrams (left) and firing times (right) for $D_{\text{star}} = 0$, $D_{\text{ring}} = 0.008$ under electromagnetic radiation intensities $k = 0.001$ and $k = 0.008$.

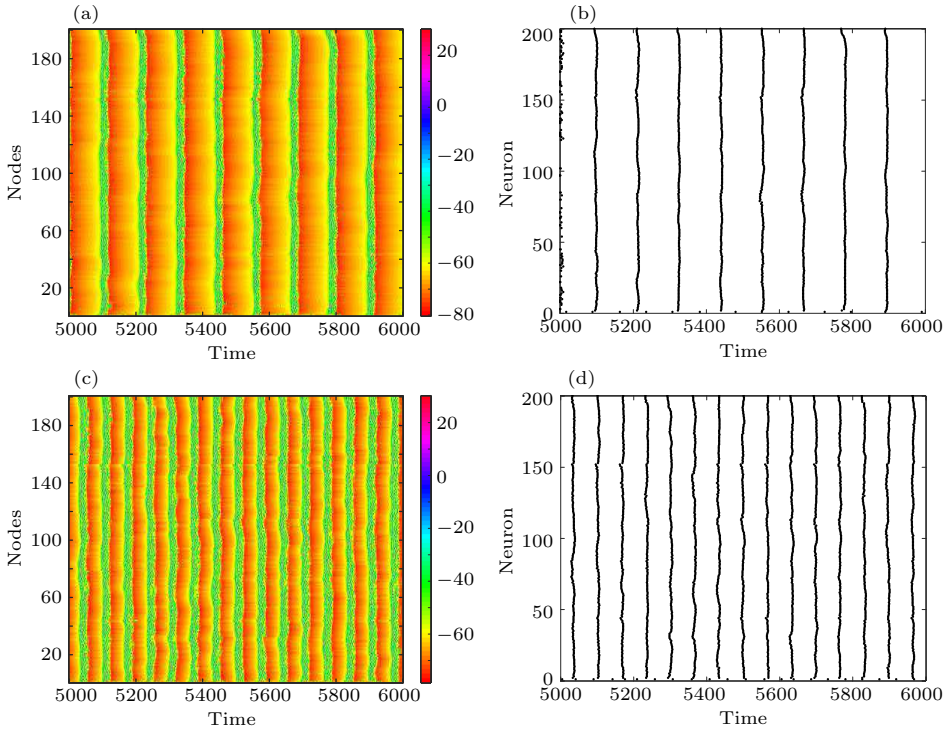


Fig. 8. Spatiotemporal diagrams (left) and firing times (right) of the RS-SWNN with coupling strength $D_{\text{star}} = 0$, $D_{\text{ring}} = 0.065$ and electromagnetic radiation strengths $k = 0.001$ and $k = 0.008$.

In summary, the experimental results validate the decisive role of the ring coupling strength D_{ring} on network synchronization. Although electromagnetic radiation exerts a certain modulating effect on the firing rhythm, its influence is relatively weak under strong ring coupling, and the neurons still maintain a high degree of synchronized firing.

For neural networks, the electromagnetic radiation effect can be regarded as an external perturbation. Under weak coupling conditions (e.g., $D_{\text{ring}} = 0.001$), the connections between neurons are relatively loose, and neurons fire independently based on their intrinsic properties. Consequently, even a slight external perturbation (such as an electromagnetic radiation intensity of ($k = 0.001$) can easily disrupt the original firing activity of neurons, leading to desynchronization

in the RS-SWNN in mode-I. As D_{ring} increases, the connections between neurons become tighter. At this stage, D_{ring} first disrupts the original firing activities of neurons, leading the network into an asynchronous state. Under these conditions, the role of electromagnetic radiation is not merely an external disturbance; it may also act as an "external coordinating signal". When k increases ($k = 0.01$), even when intrinsic coupling is insufficient to establish global synchronization, as a driving term, electromagnetic radiation can adjust the firing frequency of neurons and help the firing behavior of neurons in the network to become consistent. Consequently, the RS-SWNN in mode-I exhibits improved synchronization. However, when the coupling strength D_{ring} is sufficiently strong (e.g., $D_{\text{ring}} = 0.065$), the tight coupling between neurons is sufficient to resist external disturbances. Regardless of the variations in electromagnetic radiation intensity k, the synchronization of the neuronal network remains unchanged. Additionally, it can be observed that as the k value continues to increase, neuronal firing activity in the RS-SWNN in mode-I becomes more frequent, regardless of the coupling strength D_{ring}. This phenomenon is closely related to the Izhikevich neuron model. As the value of k increases, it simultaneously enhances the input signals to neurons, making the neuronal membrane potential more active, thereby promoting neurons to generate action potentials at a higher frequency. Table 2 summarizes the regulating effect of electromagnetic induction on network synchronization behavior.

Table 2. Impact of electromagnetic radiation on RS-SWNN synchronization.

Coupling strength	Electromagnetic radiation k	Observations & conclusions
$D_{\text{ring}} = 0.001$	$k = 0.001$	Weak radiation disrupts synchronization; network becomes asynchronous. Neuronal firing frequency remains stable.
	$k = 0.01$	Network remains asynchronous, but neuronal firing frequency increases significantly.
$D_{\text{ring}} = 0.008$	$k = 0.001$	Synchronization behavior similar to the no-radiation case.
	$k = 0.008$	Synchronization significantly improves; neurons exhibit highly aligned firing times.
$D_{\text{ring}} = 0.065$	$k = 0.001$	Network maintains high synchronization; radiation has minimal impact.
	$k = 0.008$	Neuronal firing frequency increases, but synchronization remains unaffected.

4. Conclusion

This paper proposes the RS-SWNN for the first time and studies its dynamic behavior according to different settings of coupling strengths D_{ring} and D_{star}. Unlike existing research, in the RS-SWNN in mode-I, as D_{ring} increases, it first disrupts the original firing activity of neurons, then establishes new firing behavior, and eventually leads to synchronization. In the RS-SWNN in mode-II, although an increase in D_{star} can disrupt the firing activity of neurons, it does not further promote synchronization. In the RS-SWNN in mode-III, D_{ring} plays a decisive role in determining the synchronization of the network. Moreover, this paper also investigates the effects of electromagnetic radiation on the network and analyzes how electromagnetic radiation modulates network synchronization under different coupling strengths. Although these findings provide valuable insights into the study of synchronization mechanisms in neural networks, the network size is fixed at $N = 200$, which may limit the generalizability of the findings to larger-scale networks. Furthermore, because no noise modeling was performed, the potential effects of environmental fluctuations are ignored. Going forward, we expect that integrating various methods and perspectives will enhance the understanding of synchronization dynamics in complex neural systems.

Acknowledgements

This work was supported by the Key Projects of Hunan Provincial Department of Education (Grant No. 23A0133) and the National Natural Science Foundation of China (Grant No. 62171401).

References

[1] Yuste R, Cossart R and Yaksi E 2024 *Neuron* **112** 875
[2] Bashir F, Alzahrani A, Abbas H and Zahoor F 2025 *ACS Applied Electronic Materials* **7** 1329
[3] He S B, Peng Y, Wang H, Li C and Ma M 2025 *Nonlinear Dyn.*
[4] Hodgkin A L and Huxley A F 1952 *The Journal of Physiology* **117** 500
[5] Izhikevich E M 2003 *IEEE Transactions on Neural Networks* **14** 1569
[6] Kim J, Choi Y I, Sohn J W, Kim S P and Jung S J 2023 *Experimental Neurobiology* **32** 157
[7] Vivekanandhan G, Hamarash I I, Ali Ali A M, He S and Sun K 2022 *Euro. Phys. J. Spec. Top.* **231** 4017
[8] Aristides R P and Cerdeira H A 2024 *Phys. Rev. E* **109** 044213
[9] Faci-Lázaro S, Soriano J, Mazo J J and Gómez-Gardeñes J 2023 *Chaos, Solitons & Fractals* **172** 113547
[10] Chua L 2003 *IEEE Transactions on Circuit Theory* **18** 507
[11] Strukov D B, Snider G S, Stewart D R and Williams R S 2008 *Nature* **453** 80
[12] Wan Q, Yang Q, Liu T, Chen C and Shen K 2024 *Chaos, Solitons & Fractals* **189** 115584
[13] Qin M, Lai Q, Fortuna L and Zhao X W 2025 *Nonlinear Dyn.* **113** 17095
[14] Zhang S, Wang C, Zhang H and Lin H 2024 *Chaos, Solitons & Fractals* **186** 115191
[15] Luo D, Wang C, Deng Q and Sun Y 2025 *Nonlinear Dyn.* **113** 5811
[16] Yang F, Ren G and Tang J 2023 *Nonlinear Dyn.* **111** 21917
[17] Lai Q and Yang L 2023 *Chaos, Solitons & Fractals* **174** 113807
[18] Kong X, Yu F, Yao W, Cai S, Zhang J and Lin H 2024 *Neural Networks* **171** 85

[19] Vignesh D, Ma J and Banerjee S 2024 *Neurocomputing* **564** 126961
[20] Yu F, He S, Yao W, Cai S and Xu Q 2025 *IEEE Transactions on Computer-Aided Design of Integrated Circuits and Systems*
[21] Wang H, Chen H, Sun K, Zhu W and Yao Z 2025 *Nonlinear Dyn.* **113** 10365
[22] Deng Q, Wang C, Sun Y, Deng Z and Yang G 2024 *IEEE Transactions on Circuits and Systems I: Regular Papers.* **72** 300
[23] Yu F, Zhang S, Su D, Wu Y, Gracia Y M and Yin H 2025 *Fractal and Fractional* **9** 115
[24] Lai Q, Yang L, Hu G, Guan Z H and Iu H H C 2024 *IEEE Transactions on Cybernetics* **54** 4039
[25] Paprocki B, Pregowska A and Szczepanski J 2024 *IEEE Access* **12** 42701
[26] Bashir F, Alzahrani A, Abbas H and Zahoor F 2025 *ACS Applied Electronic Materials* **7** 1329
[27] Gökgöz B, Gül F and Aydın T 2024 *Concurrency and Computation: Practice and Experience* **36** e7997
[28] Chen C, Min F, Zhang Y and Bao H 2023 *Chaos, Solitons & Fractals* **167** 113068
[29] Yuan Z, Wu Y, Ou C, Zhong P, Zhao X and Ma M 2025 *Chinese Journal of Physics* **94** 108
[30] Farrera-Megchun A, Padilla-Longoria P, Santos G J E, Espinal-Enríquez J and Bernal-Jaquez R 2024 *Chaos, Solitons & Fractals* **187** 115461
[31] Zhang J, Bao H, Gu J, Chen M and Bao B 2024 *Chaos, Solitons & Fractals* **185** 115157
[32] An X, Jiang L, Xiong L, Zhang J and Li X 2024 *Nonlinear Dyn.* **112** 16389
[33] Liao Z, Ouyang J and Ma M 2025 *Nonlinear Dyn.* **113** 12151
[34] Tang J X, Wu Y L, Ou C Y, Zhong P, Zhao X and Ma M L 2025 *Integration* **102** 102387
[35] Prasina A, Pandi V S, Nancy W, Thilagam K, Veena K and Muniyappan A 2025 *Applied Mathematics and Computation* **489** 129163
[36] Seoane J M, Bashkirtseva I, Ryashko L and Sanjuán M A F 2024 arXiv:2407.18922 [q-bio.NC]
[37] Yan Y, Liu G, Cai H, Wu E Q, Cai J, Cheok A D, Liu N, Li T and Fan Z 2024 *Neurocomputing* **599** 128098)
[38] Chauhan K, Neiman A B and Tass P A 2024 *PLoS Computational Biology* **20** e1012261
[39] Zhang J and Li Z J 2024 *Nonlinear Dyn.* **112** 6647
[40] Ma M L and Lu Y P 2024 *Chaos* **34** 033116
[41] Njitacke Z T, Tsafack N, Ramakrishnan B, Rajagopal K, Kengne J and Awrejcewicz J 2021 *Chaos, Solitons & Fractals* **153** 111577
[42] Muni S S, Rajagopal K, Karthikeyan A and Arun S 2022 *Chaos, Solitons & Fractals* **155** 111759
[43] Yang H, Tian S, Zhu H and Xu G 2023 *Journal of Biomedical Engineering* **40** 859